

Boundary Energies and the Geometry of Phase Separation in Double-Exchange Magnets

D. I. Golosov* and D. Orgad

Racah Institute of Physics, The Hebrew University, Jerusalem 91904, Israel.

(Dated: October 18, 2018)

We calculate the energy of a boundary between ferro- and antiferromagnetic regions in a phase separated double-exchange magnet in two and three dimensions. The orientation dependence of this energy can significantly affect the geometry of the phase-separated state in two dimensions, changing the droplet shape and possibly stabilizing a striped arrangement within a certain range of the model parameters. A similar effect, albeit weaker, is also present in three dimensions. As a result, a phase-separated system near the percolation threshold is expected to possess intrinsic hysteretic transport properties, relevant in the context of recent experimental findings.

PACS numbers: 75.47.Gk, 75.30.Kz, 75.10.Lp

Phase separation is ubiquitous in systems involving multiple types of degrees of freedom and opposing interactions. Among the growing number of compounds which are known to exhibit experimental signatures consistent with this phenomenon one finds the doped manganese oxides^{1,2} [renowned due to their colossal magnetoresistance (CMR)], as well as lightly-doped magnetic semiconductors¹ (*e.g.*, Eu-based). The basic physics of both of these systems involves conduction electrons that hop between sites in a crystal, whose ionic (localized) core spins are coupled to the electronic spins via a strong on-site ferromagnetic Hund's exchange interaction. Under broad conditions, the energy of the Fermi sea of conduction electrons is then minimized when the core spins are ordered ferromagnetically, giving rise to *double-exchange* ferromagnetism³. This ordering is opposed by strong antiferromagnetic tendencies present in such systems, which originate from Heisenberg superexchange between the core spins, and which may also be complemented by other, band-structure and orbital-related, mechanisms. Phase separation resolves this competition by dividing the system into regions of different magnetic orders and electronic band-widths. We will be concerned with the case where the ferromagnetic regions in which the electrons are free to move (and thereby to lower their kinetic energy) co-exist with electron-poor domains where antiferromagnetism prevails.

The present article focuses on the properties of the boundaries between different regions in the sample. It is shown that with increasing strength of antiferromagnetism the boundary energy becomes increasingly dependent on the orientation of the boundary with respect to the lattice. Thus, when the Eu chalcogenides (which have Néel temperatures of the order of 10 K or below) are doped with carriers, the latter are predicted to form droplets of circular or spherical shape. In the CMR manganates, on the other hand, antiferromagnetism is much more pronounced and we expect a strong dependence of the boundary energy on orientation. This fact, in turn, is likely to contribute to the unusual transport properties of the CMR manganates near percolation threshold including hysteresis, memory and switching effects^{4,5}.

Although to the best of our knowledge such considerations have not been presented before, it appears reasonable to expect that at the qualitative level these are not specific for the simplified model considered below, nor indeed for double-exchange magnetism. Support for this view can be drawn from the numerical studies of phase separation in the $t - J$ and Hubbard models, showing diamond-shaped islands⁶ or an anisotropy in the stripe direction⁷. Rigorous results on the preferred wall direction between ferromagnetic domains in the Falicov-Kimball model⁸ are likely to be indicative also of the behavior of phase separation boundaries in this model.

We begin with the standard double-exchange Hamiltonian,

$$\mathcal{H} = -\frac{t}{2} \sum_{\langle i,j \rangle, \alpha} \left(c_{i\alpha}^\dagger c_{j\alpha} + c_{j\alpha}^\dagger c_{i\alpha} \right) - \frac{J_H}{2S} \sum_{i, \alpha, \beta} \vec{S}_i \vec{\sigma}^{\alpha\beta} c_{i\alpha}^\dagger c_{i\beta} + \frac{J}{S^2} \sum_{\langle i,j \rangle} \vec{S}_i \vec{S}_j. \quad (1)$$

Here $c_{j\alpha}$ ($\alpha = \uparrow, \downarrow$) are the electron annihilation operators, \vec{S}_i are the operators of the core spins located at the sites of a square (or simple cubic) lattice, and the vector $\vec{\sigma}^{\alpha\beta}$ is composed of Pauli matrices. The ionic spins, which are treated classically (assuming $S \gg 1$), interact with each other via a nearest-neighbor superexchange J and with the spins of the conduction electrons via a large Hund's coupling J_H . We consider the limit⁹ $J_H \rightarrow \infty$ and omit all peculiarities of lattice and orbital structure (which vary between compounds). While the long-range Coulomb interaction is absent from the Hamiltonian its effects will be discussed qualitatively. Throughout this paper we assume zero temperature and take the lattice spacing, the bare hopping amplitude t , and \hbar to be 1. Since the resulting model is symmetric with respect to quarter-filling $x = 0.5$, we treat the $x < 0.5$ case only.

As $J_H \rightarrow \infty$, there is only one spin state available for a conduction electron at each lattice site. The carriers can therefore be treated as spinless, and their nearest-neighbor hopping amplitude depends on the local spin configuration via the double-exchange mechanism¹⁰. In

particular, it equals 1 when the ionic spins at the two neighboring sites are parallel to each other, and it vanishes in the case of anti-parallel spins. When a certain number of carriers, $N_e = xN$, where N is the number of sites in the system, are doped into an insulating (antiferromagnetic) double-exchange magnet, it proves energetically favorable for all these carriers to concentrate in one part of the sample. The magnetic ordering in this part is changed to a ferromagnetic one, while the rest of the sample remains antiferromagnetic and free of conduction electrons (as long as x and J are not too large, see below). The optimal value of the carrier concentration in the ferromagnetic region, $x_{FM} > x$, is determined by the condition

$$\Omega_{AFM} = \Omega_{FM} , \quad (2)$$

where in the case of dimensionality D the thermodynamic potentials of the antiferromagnetic and ferromagnetic phases are given by $\Omega_{AFM}(J) = -DJ$ and $\Omega_{FM}(J, \mu) = \int_{-D}^{\mu} (\epsilon - \mu) \nu_D(\epsilon) d\epsilon + DJ$. Here the chemical potential is denoted by $\mu - J_H/2$ and $\nu_D(\epsilon)$ is the density of states for the 2D (3D) tight-binding electronic dispersion, $\epsilon_{\vec{k}} = -\cos k_x - \cos k_y (-\cos k_z)$.

The values of μ and $x_{FM} = \int_{-D}^{\mu} \nu_D(\epsilon) d\epsilon$ depend solely on J (see the dotted lines in Fig. 2 below). When the value of the nominal density x reaches $x_{FM}(J)$, the entire sample turns ferromagnetic. However, an investigation of the energy balance and stability of different phases shows that thermodynamic equilibrium between Néel and ferromagnetic phases is possible only as long as x_{FM} is not too large, $x_{FM} < x_c$ or equivalently $J < J_c$. While the precise value of J_c is not known, a variational study¹¹ in 2D shows that $x_c < 0.245$, corresponding to $J_c < 0.036$. In 3D, $x_c < 0.291$ or $J_c < 0.035$, at which point the spin stiffness in the ferromagnetic phase turns negative. If the value of J exceeds J_c the magnetic ordering in either the electron-rich or the electron-poor regions of the sample will differ from that of a ferromagnet or a Néel antiferromagnet. Rather, one of the many possible antiferromagnetic phases characterized by non-vanishing conduction electron density may be stabilized (see Ref. 11 for examples). Throughout the present article, we assume that J is smaller than J_c .

The presence of phase separation inevitably raises questions regarding the structure of the boundary between the phases. In an earlier article¹¹, it was suggested that the most energetically favorable structure of such a boundary corresponds to an abrupt change in the magnetic order. For the case of phase separation into ferromagnetic and Néel phases, which is of interest to us here, straight boundaries running in the direction of a lattice diagonal in a 2D system were considered [see Fig. 1 (a)]. The energy of such a boundary per unit length is given by¹²

$$\sqrt{2}W_d^{(2D)}(J) = \frac{\sqrt{4 - \mu^2}}{2\pi} - \frac{|\mu|}{2\pi} \arccos \frac{|\mu|}{2} - \mu x_{FM} \quad (3)$$

$$- \frac{4}{\pi^2} \mathcal{E} \left(\sqrt{1 - \frac{\mu^2}{4}} \right) + \frac{\mu^2}{\pi^2} \mathcal{K} \left(\sqrt{1 - \frac{\mu^2}{4}} \right),$$

where \mathcal{K} and \mathcal{E} are the elliptic integrals¹³.

In 3D, the analogue of such an abrupt diagonal boundary is an abrupt planar boundary perpendicular to a main diagonal [direction (1, 1, 1) or equivalents] of the cubic lattice. The calculations of Ref. 12 can be generalized to the 3D case, yielding the boundary energy,

$$W_d^{(3D)} = \frac{1}{8} \int [\mu + \lambda(\vec{k}_{\perp})] \theta \left(\mu + \lambda(\vec{k}_{\perp}) \right) \frac{d^2 k_{\perp}}{4\pi^2} - 2\sqrt{3}J, \\ \lambda^2(\vec{k}_{\perp}) = 3 + 2 \cos k_1 + 4 \cos \frac{\sqrt{3} k_2}{2} \cos \frac{k_1}{2}, \quad (4)$$

per unit area. In Eq. (4), the integration variable $\vec{k}_{\perp} = \{k_1, k_2\}$ varies over the first Brillouin zone of a triangular lattice of unit spacing. The k_1 axis is chosen in one of the nearest-neighbor directions.

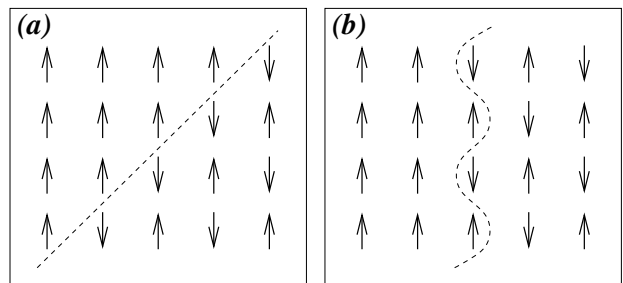


FIG. 1: Diagonal (a) and vertical (b) boundaries in the 2D case.

In the case of small $J \ll 1$, these somewhat cumbersome expressions reduce to

$$W_d \approx \begin{cases} \frac{4\sqrt{2}}{3\pi^{1/4}} J^{3/4} - 2\sqrt{2}J & \text{in 2D,} \\ \frac{3^{8/5} 5^{4/5}}{16 \cdot 2^{2/5}} \pi^{3/5} J^{4/5} - 2\sqrt{3}J & \text{in 3D.} \end{cases} \quad (5)$$

In both 2D (Refs. 11,13) and 3D cases, one can verify that tilting the spins adjacent to a diagonal boundary (effectively spreading it over two or three lattice links) increases the boundary energy. This strongly supports the notion of an abrupt inter-phase boundary. The fact that the boundary is sharp (as opposed to a smooth Bloch-like wall) implies the absence of a continuum limit and hence a non-trivial dependence of the boundary energy on orientation. We will now explore this property variationally in more detail.

Specifically, we consider a boundary running perpendicularly to the (1, 0) and (1, 0, 0) directions in the 2D [Fig.1 (b)] and 3D cases, respectively. The energy of such a “vertical” wall in $D = 2, 3$ dimensions can be evaluated exactly within the same technique (see Appendix). We find

$$W_v = \frac{1}{2} \int_{1-D}^0 \nu_{D-1}(\epsilon_{\perp}) d\epsilon_{\perp} \int_{-D}^{\mu(J)} \xi(\epsilon, \epsilon_{\perp}) d\epsilon - DJ. \quad (6)$$

Assuming that $\epsilon < 0$, the spectral shift function $\xi(\epsilon, \epsilon_{\perp})$ is given by

$$\xi = \begin{cases} 0, & \epsilon_{\pm} < -Q \\ \frac{1}{2} - \frac{2}{\pi} \arctan \frac{\sqrt{Q^2 - \epsilon_{\pm}^2}}{\sqrt{\epsilon_{\pm}^2 - Q^2 - 2\epsilon}}, & \epsilon_{-} < -Q < \epsilon_{+} < Q \\ 1 - \frac{2}{\pi} \arctan \frac{\sqrt{Q^2 - \epsilon_{+}^2} + \sqrt{Q^2 - \epsilon_{-}^2}}{-2\epsilon}, & -Q < \epsilon_{\pm} < Q \\ 1, & \epsilon_{-} < -Q, \epsilon_{+} > Q \end{cases} \quad (7)$$

where in the present case $Q = 1$ and $\epsilon_{\pm} = \epsilon \mp \epsilon_{\perp}$.

At small J , one obtains

$$W_v \approx \begin{cases} \frac{4\sqrt{2}}{3\pi^{1/4}} J^{3/4} - (4 - \sqrt{2})J & \text{in 2D,} \\ \frac{3^{8/5} 5^{4/5}}{16 \cdot 2^{2/5}} \pi^{3/5} J^{4/5} - (6 - \sqrt{6})J & \text{in 3D.} \end{cases} \quad (8)$$

The leading-order terms in Eqs. (5) and (8) originate from the energy of a partition inserted into an ideal gas of electrons. In the limit of small J (corresponding to small x_{FM} and to a large Fermi wavelength) this quantity should not depend on the orientation of the partition with respect to the lattice, as is manifest from Eqs. (5) and (8). This independence of the boundary energy on orientation at small J is expected to hold generally, and not only for the two directions considered above. The droplets of a ferromagnetic phase within an antiferromagnetic sample will then have a circular (spherical) shape, obtained by minimizing the boundary length or area¹⁴. This changes with increasing J as we discuss below.

The 2D case. The energy of a vertical boundary always exceeds that of the diagonal one [see Fig. 2 (a)], and with increasing J the ratio $w = W_v/W_d$ increases. The droplet shape in 2D then approaches that of a diamond with rounded corners. The curvature radii at the corners decrease as w increases. We model this transition approximately, allowing only for the vertical and diagonal orientations of the boundary (see Fig. 3). Minimizing the boundary energy of the droplet with respect to the ratio α of the combined length of the vertical components to that of the diagonal ones while keeping the area of the droplet constant yields $\alpha = (\sqrt{2} - w)/(\sqrt{2}w - 1)$. As the value of w increases from 1 to $\sqrt{2}$ (the latter corresponds to $J \approx 0.030$ or $x_{FM} \approx 0.221$), the droplet shape changes from that of a regular octagon¹⁵ to that of a diamond.

This conclusion is expected to affect the properties of the system in a case where the ferromagnetic phase occupies a considerable fraction of the sample. The long-range Coulomb interaction dictates that instead of a single charged macroscopic droplet of a ferromagnet, a Wigner crystal-like array of smaller droplets is formed¹⁶. Provided that these droplets are large enough¹⁴ and well separated in space, the shape of each droplet is governed by the results reported above. The small- J regime of $w - 1 \ll 1$, and hence circular droplets, is predicted for Eu-based semiconductors¹. As more carriers are doped into such a system, the geometry of the state eventually changes from that of disconnected droplets of a (metallic)

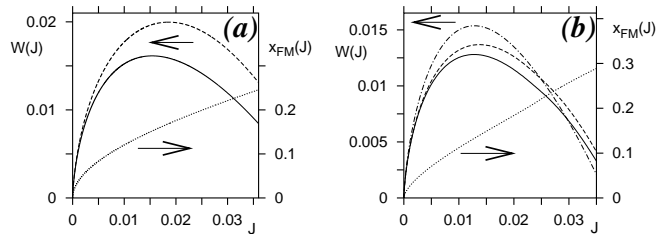


FIG. 2: The dependence of the diagonal, vertical, and [in (b)] {110} boundary energies (solid, dashed, and dashed-dotted lines, respectively) on the value of the superexchange coupling J in the 2D (a) and 3D (b) cases. Dotted lines (right scale) show the carrier density $x_{FM}(J)$ in the ferromagnetic regions.

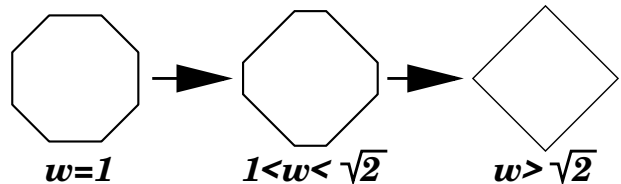


FIG. 3: Evolution of the droplet shape in the 2D case.

ferromagnet embedded in an antiferromagnetic insulator to the inverse situation of a connected metallic phase¹.

The regime of larger $J \gtrsim 0.015$ is expected to be realized in the CMR manganates¹⁷. The corresponding w exceeds 1.25, leading to the following consequences:

(i) *Hysteretic effects in transport.* When the ferromagnetic droplets are not connected an applied voltage gives rise to internal electrostatic fields. Connected conduction paths could then form in order to lower the associated field energy. When subsequently the voltage is applied along another direction, these paths should restructure accordingly. Due to the dependence of the boundary energy on orientation, this cannot occur smoothly, but necessarily involves discrete transitions (over energy barriers) and hysteresis. Experimentally, switching and memory effects in the resistivity of CMR manganates near the percolation threshold have been observed both in thin films⁵ and in 3D single crystals⁴. We emphasize that such properties arise here as intrinsic to the system, as opposed to more conventional effects of impurity pinning of the boundary.

(ii) For a fixed area fraction of the ferromagnet, x/x_{FM} , the ratio $\Lambda = (\Omega_s - \Omega_{dr})\sqrt{\epsilon}/(e^2W_d)^{1/2}$, where Ω_{dr} and Ω_s are the energies of a droplet phase and of a phase composed of diagonal ferro- and antiferromagnetic stripes, depends solely on the droplet geometry¹² (here, ϵ is the dielectric constant). Variational studies^{1,12} suggest that for $w = 1$ (circular droplets) and $x/x_{FM} \approx 1/2$ the quantity Λ is only slightly larger than 0. While leaving this issue for future study, we note that since $\Omega_{dr}\sqrt{\epsilon}/(e^2W_d)^{1/2}$ is expected to be larger for diamond-shaped droplets (due to a higher value of boundary en-

ergy per particle), it is possible that for large w a *diagonal stripe phase* proves energetically favorable ($\Lambda < 0$) in a region near $x/x_{FM} = 1/2$. In a broader physical context, droplet shape effects may complement other mechanisms suggested¹⁸ to stabilize a stripe phase in the CMR manganates.

The 3D case. As seen from Fig. 2 (b), the energies of the vertical and diagonal boundaries follow each other closely (with $W_d > W_v$ for $J < 0.00019$) throughout the relevant range of the values of J . Thus, using the same arguments as above (cf. Fig. 3) we conclude that the optimal droplet shape remains close to that of an octahedron (formed by diagonal boundaries) with its vertices “shaved off” by vertical and horizontal planes. Energetically, this geometry is nearly indistinguishable from that of a sphere. In such a case, one can expect based on the variational results for spherical droplets^{1,19} that an alternating arrangement of ferro- and antiferromagnetic planar slabs is unstable for all values of x/x_{FM} . However, the boundary energy even in 3D is not at all orientation-independent. This is illustrated by the dashed-dotted line in Fig. 2 (b), which shows the energy W_{110} of a boundary perpendicular to the (1,1,0) direction²⁰,

$$W_{110} = \frac{1}{2\sqrt{2}} \int_{-\pi}^{\pi} \frac{dk_y}{2\pi} \int_{-\pi/2}^{\pi/2} \frac{dk_z}{2\pi} \int_{-3}^{\mu} \xi(\epsilon, k_y, k_z) d\epsilon - \frac{3J}{\sqrt{2}}. \quad (9)$$

Here, the function ξ is given by Eq. (7) with $Q = 2 \cos(k_y/2)$ and $\epsilon_{\pm} = \epsilon \pm \cos k_z$. At small J , we find

$$W_{110} \approx \frac{3^{8/5} 5^{4/5}}{16 \cdot 2^{2/5}} \pi^{3/5} J^{4/5} - \frac{6 - \sqrt{3}}{\sqrt{2}} J. \quad (10)$$

As illustrated by Fig. 2 (b), W_{110} exceeds both W_d and W_v by some 20% in an extended range of values of J . Thus, our conclusion on hysteresis due to abrupt switching of the conduction paths *persists in 3D* (at least for some directions of the path). This has an enhanced significance because in 3D, point defects are less likely to interfere with the restructuring of conduction paths.

We note that in a phase-separated system quenched (chemical) disorder that leads to variations in the on-site energies also tends to sub-divide large ferromagnetic areas into droplets. Since the boundary energy originates from an integral of the carrier phase shift over the entire Fermi sea, it is expected to be only weakly sensitive to the detailed structure of individual wavefunctions (as long as the disorder is not too strong). Hence, we expect the orientational dependence of the boundary energy to persist in the presence of such inhomogeneities (and of many-body effects due to the short-range part of the Coulomb interaction⁹). This is illustrated by numerical-simulation results for a 2D phase-separated double-exchange magnet with disorder²¹, showing that the prevailing direction of the boundaries is clearly along the diagonals.

We note that in order to make quantitative comparison with the experimental results for the manganates one may have to complement Eq. (1) with further terms re-

flecting orbital and lattice effects inherent to these compounds. While these may affect the optimal shape or the preferred direction of the boundaries in a phase separated system, our overall conclusion on the presence of an orientational dependence of the boundary energy is expected to persist. As demonstrated above for the simple model (1), this general conclusion follows from the presumed short-wavelength (abrupt) nature of the boundary, combined with sufficiently large band-filling. The latter ensures that the short-wavelength (on the scale of the lattice constant) properties of the electron gas are sensitive to the orientation with respect to the lattice. Including phonon or orbital degrees of freedom may modify this short wavelength behavior, but is rather unlikely to eliminate it altogether.

As we have previously mentioned, experimental observations of non-ohmic behavior and memory effects in the resistivity of CMR manganates near the percolation threshold exist both for 3D single crystals⁴ and for thin films⁵. While qualitatively this is in line with our expectations, it would be desirable to have direct imaging of the spatial structure of the underlying phase-separated state (as provided by magnetic force microscopy). Such measurements could also be used to search for any putative stripe phases, especially in 2D. We are not aware of similar transport studies of the Eu-based magnetic semiconductors, and indeed we do not expect intrinsic nonlinear effects to be prominent in this case. However, this point should also be confirmed by experiments.

We acknowledge helpful discussions with O. Agam, G. Jung, and V. Markovich, as well as the support of the ISF (under the Centers of Excellence Program), the BSF (grant No. 2004162), and the Israeli Absorption Ministry.

APPENDIX

In the following we briefly outline the calculation of the “vertical” boundary energy, Eqs. (6–7) using the theory of local perturbations due to I. M. Lifshits and M. G. Krein²². We first evaluate the double-exchange (electronic kinetic energy) contribution to the boundary energy. The (auxiliary) unperturbed system consists of two disconnected components:

(i) A square (in 3D, cubic) tight-binding network of N sites, which we divide into two sub-lattices, labeled b and c (see Fig. 4), thereby doubling the period in the direction perpendicular to the x axis (in 3D, this corresponds to a checkerboard arrangement in the yz plane). Performing a partial Fourier transform in the y (in 3D, y and z) direction, renders the Hamiltonian as

$$\mathcal{H}_1 = \sum_{x, \vec{k}_{\perp}} \left[-\frac{1}{2} b_{\vec{k}_{\perp}}^{\dagger}(x) b_{\vec{k}_{\perp}}(x+1) - \frac{1}{2} c_{\vec{k}_{\perp}}^{\dagger}(x) c_{\vec{k}_{\perp}}(x+1) + \epsilon_{\perp}(\vec{k}_{\perp}) c_{\vec{k}_{\perp}}^{\dagger}(x) b_{\vec{k}_{\perp}}(x) + \text{H.c.} \right], \quad (\text{A.1})$$

where the operators b and c annihilate the two species of spinless fermions on the two sub-lattices, and $\epsilon_{\perp}(\vec{k}_{\perp}) = -\cos k_y (-\cos k_z)$ is the usual tight-binding dispersion in $D - 1$ dimensions.

(ii) A chain of \sqrt{N} sites (for the 3D case, a plane of $N^{2/3}$ sites), disconnected from each other (zero hopping amplitudes, hence $\mathcal{H}_2 = 0$). We again introduce two sub-lattices in a checkerboard fashion, and perform the Fourier transform, labeling the two resulting localized fermion operators f and g with the $D - 1$ -dimensional momentum index, \vec{k}_{\perp} .

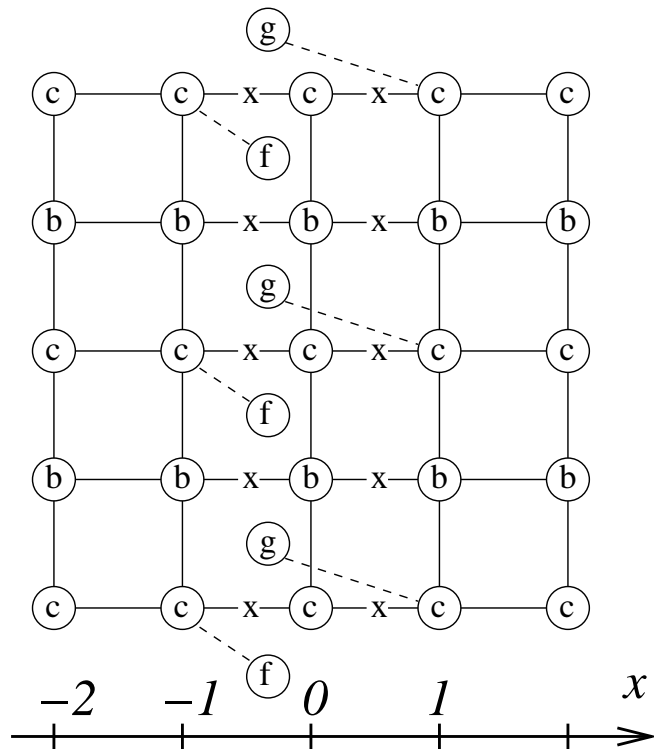


FIG. 4: The effect of the perturbation, Eq. (A.2), in the 2D case. Carrier hopping along the lattice links marked “x” is eliminated, and the new bonds (dashed lines) are established.

Next, consider a perturbation of the form

$$V = \frac{1}{2} \sum_{\vec{k}_{\perp}} \left\{ b_{\vec{k}_{\perp}}^{\dagger}(0) [b_{\vec{k}_{\perp}}(1) + b_{\vec{k}_{\perp}}(-1)] + c_{\vec{k}_{\perp}}^{\dagger}(0) [c_{\vec{k}_{\perp}}(1) + c_{\vec{k}_{\perp}}(-1)] - f_{\vec{k}_{\perp}}^{\dagger} c_{\vec{k}_{\perp}}(-1) - g_{\vec{k}_{\perp}}^{\dagger} c_{\vec{k}_{\perp}}(1) + \text{H.c.} \right\}. \quad (\text{A.2})$$

The first two terms correspond to disconnecting the $x = 0$ chain (plane) from the rest of the system. An extra site is then connected to every other site at $x = \pm 1$ (last two terms in V), creating a vertical boundary perpendicular to the x axis (see Fig. 4). Note that hopping is allowed both in the right, and in the left half-plane

(half-space). Therefore, the change in energy of the system due to the perturbation (when supplemented with the appropriate superexchange contribution) is equal to twice the energy of a vertical boundary between an antiferromagnet (where the hopping amplitude vanishes) and a ferromagnet, as pictured in Fig. 1 (b).

Since the transverse momentum \vec{k}_{\perp} is preserved by V , the variables separate. For a given \vec{k}_{\perp} , the perturbation is localized at $x = 0, \pm 1$ and takes the form

$$V_{\vec{k}_{\perp}} = \sum_{i=1}^6 A_i a_i^{\dagger} a_i, \quad (\text{A.3})$$

where $2A_i = \{-\sqrt{3}, -1, 1, \sqrt{3}, -\sqrt{2}, \sqrt{2}\}$ and a_i are suitable combinations of the original fermion operators that satisfy $a_i a_j^{\dagger} + a_j^{\dagger} a_i = \delta_{ij}$. The spectral shift function, Eq. (7), is then evaluated as²²

$$\xi(k_{\perp}, \epsilon) = -\frac{1}{\pi} \text{Arg Det} \{ \hat{1} - M_{ij} A_j \}, \quad (\text{A.4})$$

with

$$M_{ij} = \int \frac{dk_x}{2\pi} \left[\frac{\langle a_i | p_k^{\dagger} \rangle \langle p_k^{\dagger} | a_j \rangle}{\epsilon_+ + \cos k_x - i0} + \frac{\langle a_i | p_k^- \rangle \langle p_k^- | a_j \rangle}{\epsilon_- + \cos k_x - i0} \right] + \frac{\langle a_i | f_{\vec{k}_{\perp}} \rangle \langle f_{\vec{k}_{\perp}} | a_j \rangle + \langle a_i | g_{\vec{k}_{\perp}} \rangle \langle g_{\vec{k}_{\perp}} | a_j \rangle}{\epsilon - i0}. \quad (\text{A.5})$$

Here, the Dirac bra and ket states are defined by $|f_{\vec{k}_{\perp}}\rangle = f_{\vec{k}_{\perp}}^{\dagger} |0\rangle$ (with $|0\rangle$, the vacuum state), etc., and the operators p_k^{\pm} are the Fourier components (with respect to k_x) of $(c_{\vec{k}_{\perp}}(x) \pm b_{\vec{k}_{\perp}}(x))/\sqrt{2}$. As before $\epsilon_{\pm} = \epsilon \mp \epsilon_{\perp}(\vec{k}_{\perp})$.

The choice of the Arg branch in Eq. (A.4) is subject to the requirement that $\xi(k_{\perp}, \epsilon) \rightarrow 0$ for a vanishing perturbation strength, *e.g.*, if the Hamiltonian is given by $\mathcal{H}_1 + \mathcal{H}_2 + \alpha V$ with $\alpha \rightarrow 0$. In the 3D case, we note the appearance of bound (Tamm) surface electron states at the vertical border. These have the energy $E = \pm \cosh(k_x) + \epsilon_{\perp} = 0$ with $|\epsilon_{\perp}(\vec{k}_{\perp})| > 1$. For example the wave function of an $\epsilon_{\perp} > 1$ state in the $x < 0$ half of the system differs from zero only on the f sites ($x = 0$), on the c sites with even x , and on the b sites with odd x (see Fig. 4), where it is proportional to $\exp[k_x x + i k_y y + i k_z z]$. The net spectral shift function, Eq. (A.4), contains contributions from these boundary states, from the extended states in the two half systems and also from the states in the disconnected $x = 0$ chain/plane (see Fig. 4). The latter needs to be subtracted when calculating the desired boundary energy. The resulting $\xi(\epsilon, \epsilon_{\perp})$ is given by Eq. (7).

By counting the number of antiferromagnetic links and the associated energy change, one arrives at the final expression, Eq. (6). The energy of a $\{110\}$ boundary, Eq. (9), can be evaluated in a similar way.

-
- * Electronic address: golosov@phys.huji.ac.il
- ¹ E. L. Nagaev, *Colossal magnetoresistance and phase separation in magnetic semiconductors* (Imperial College Press, London, 2002).
 - ² E. Dagotto, *Nanoscale Phase separation and colossal magnetoresistance* (Springer, Berlin, 2003).
 - ³ P.-G. de Gennes, Phys. Rev. **118**, 141 (1960).
 - ⁴ Y. Yuzhelevski *et al*, Phys. Rev. B **64**, 224428 (2001); V. Markovich *et al*, Phys. Rev. B **70**, 064414 (2004) and Eur. Phys. J. B **48**, 41 (2005); M. Tokunaga, Y. Tokunaga, and T. Tamegai, Phys. Rev. Lett. **93**, 037203 (2004); G. Garbarino *et al*, Physica B **354**, 16 (2004).
 - ⁵ A. Biswas *et al*, Phys. Rev. B **63**, 184424 (2001); F. X. Hu and J. Gao, Phys. Rev. B **69**, 212413 (2004); A. Bhat-tacharya *et al*, Phys. Rev. B **72**, 132406 (2005).
 - ⁶ E. Eisenberg *et al*, Phys. Rev. B **65**, 134437 (2002).
 - ⁷ See, *e.g.*, R. Citro and M. Marinaro, Eur. Phys. J. B **20**, 343 (2001); M. Yu and H. Q. Lin, Int. J. Mod. Phys. B **19**, 299 (2005).
 - ⁸ N. Datta, A. Messager, and B. Nachtergaele, J. Stat. Phys. **99**, 461 (2000).
 - ⁹ In reality, J_H is finite and the strong Hubbard interaction U must be taken into account. These facts are not expected to cause a qualitative change in our results, with the main effect of U being a mean-field renormalization of the model parameters, cf. Ref. 23.
 - ¹⁰ P. W. Anderson and H. Hasegawa, Phys. Rev. **100**, 675 (1955).
 - ¹¹ D. I. Golosov, J. Appl. Phys. **91**, 7508 (2002).
 - ¹² D. I. Golosov, Phys. Rev. B **67**, 064404 (2003).
 - ¹³ We have verified all our results pertaining to the 2D case via numerical diagonalization of finite clusters.
 - ¹⁴ We assume that the Fermi wavelength in the ferromagnetic phase is much smaller than the droplet size. In this case, one can omit the effects of curvature of the boundary, corners and size-dependent quantum oscillations.
 - ¹⁵ Approximating a circle by an octagon results in a 2.7 % error in the value of the boundary energy per particle.
 - ¹⁶ The size of the droplets should not exceed the Debye-Hückel screening radius (assumed large, see Ref. 12).
 - ¹⁷ The bare J , which can be roughly estimated from the Néel temperature of fully hole-doped CMR compounds, is enhanced by inter-subband virtual hopping (cf. Ref. 23).
 - ¹⁸ Long-range elastic forces may also stabilize stripes, see D. I. Khomskii and K. I. Kugel, Europhys. Lett. **55**, 208 (2001).
 - ¹⁹ V. A. Kashin and E. L. Nagaev, Sov. Phys. JETP, **39**, 1036 (1974).
 - ²⁰ The $\{110\}$ boundary is corrugated with chains of ferromagnetically aligned spins running in the $(-1,1,0)$ direction. On the vertical $\{100\}$ boundary, ferromagnetic sites protrude in a checkerboard pattern. [cf. Fig. 1 (b)].
 - ²¹ S. Kumar and P. Majumdar, Phys. Rev. Lett. **92**, 126602 (2004), Fig. 2.
 - ²² I. M. Lifshits, Usp. Mat. Nauk **7**, No. 1, 171 (1952) (*in Russian*); I. M. Lifshits, S. A. Gredeskul, and L. A. Pastur, *Introduction to the Theory of Disordered Systems* (J. Wiley & Sons, New York, 1988), Chapt. 5.; M. G. Krein, *Topics in Differential Equations and Operator Theory* (Birkhäuser, Basel, 1983), pp. 107-172.
 - ²³ D. I. Golosov, Phys. Rev. B **71**, 014428 (2005).